https://dx.doi.org/10.21577/0103-5053.20220135

J. Braz. Chem. Soc., Vol. 34, No. 5, 653-663, 2023

Article

Sugarcane Bagasse Fibers Derivatives and Their Application in Chitosan-Based Composite Films for NPK Fertilizer Release

Lucas Luiz Messa, *,[a] *Gabriela Aparecida Contieri*[a] *and Roselena Faez* *,[a]

[a]*Laboratório de Materiais Poliméricos e Biossorventes, Universidade Federal de São Carlos (UFSCar), Campus Araras, 13600-970 Araras-SP, Brazil*

Encapsulation and release of NPK fertilizer by composite films were systematically demonstrated by casting dispersions of chitosan (CS) and sugarcane bagasse (SCB) derivatives (holocellulose (HC), cellulignin (CL), and cellulose (CEL)) fibers under varied CS-to-NPK and CS-to-SCB derivatives mass ratios. SCB derivatives were obtained from sugarcane bagasse as agricultural waste by following the alkali dissolution (4% NaOH, 70 °C for 5 min), sodium chlorite delignification (1.4% $NaClO_2$, pH 3.5, 70 °C, 5 h), or from a combination of both. Nutrient-adsorption capacity can be tunable by the chemical composition of SCB derivatives, i.e., fibers with noncellulosics exhibited higher adsorption capacities while the absence of noncellulosics lessened their adsorption capacity. Oven-drying (60 °C, 5 h) of optimal 1:0.5 CS/NPK film-forming solution produced highly uniform films with shape with 0.31 ± 0.02 mm thickness while increasing fiber content in the solution to 25 or 50% prevents films retraction effect. The release of highly water-soluble NPK fertilizer from these composite films was lower with hemicelluloses (52-82%) or lignin (55-92%) contents in SCB fiber than in noncellulosics absence (71-100%), thus could be tuned by varying the chemical composition SCB derivative, followed by a *quasi*-Fickian diffusion mechanism in water.

Keywords: agricultural residue, biopolymers, controlled-release fertilizer

Introduction

Brazil is characterized by its agricultural activity as one of the principal economic bases of the country.[1] Soil fertilization is one of the factors contributing to these criteria.[2] However, Brazilian agriculture is responsible for 7% of the world's fertilizer consumption, preceded by China, India, and the United States, with approximately 70% of the used amount being imported,[3] making the country highly dependent on imports. Additionally, chemical fertilizers are used in excessive and disproportionate quantities, resulting in fertilizer losses from 40 to 90%, causing environmental and financial adverse impacts.[4] Therefore, there is a clear need to explore new agricultural technological practices to reduce or replace the use of chemical fertilizers and, consequently, mitigate their imports.

Enhanced efficiency fertilizers (EEFs) are specifically designed formulations that control or delay the release of nutrients aiming to enhance nutrient use efficiency without suffering from agricultural input losses.[5] Over time, various materials have been explored for EEFs production. Initially, molten sulfur was tried as a coating material to reduce the immediate contact of fertilizer with its surrounding environment.[5-7] Later, research focused on polymeric materials as a more technological coating.[8-14] However, most of these EEFs need additional chemicals (i.e., sealing agents, synthetic polymers, crosslinking reagents, polymerization initiators, organic solvents, etc.) or are fabricated through complex production processes, add extra expense to the final product, and can be harmful if accumulated in the environment. In recent years, bio-based polymers such as alginate,[15,16] starch,[17-20] chitosan (CS),[21-24] polyhydroxybutyrate,[25] and cellulose[26,27] have been investigated to overcome these economic and environmental obstacles. Chitosan-based materials have garnered considerable attention due to their ability to interact with anionic species,[28,29] besides their known characteristics of biodegradability,[30-32] renewability at relatively low cost,[33] and non-toxicity.[30] However, these CS-based materials suffer from drawbacks such as poor tensile strength and insufficient elasticity.[34] Combining

*e-mail: messalucas@hotmail.com; faez@ufscar.br
Editor handled this article: Fernando C. Giacomelli

CS with other polymers could be a suitable way to solve this problem.[35]

Sugarcane bagasse (SCB), the most abundant agricultural biomass in Brazilian agriculture, could be applied as reinforcing fiber to prepare composite materials with enhanced properties due to their high content of cellulose,[36] which is characterized by being fibrillar and crystalline.[37] After cellulose (42%), hemicelluloses (28%), and lignin (22%) are the most abundant components found in SCB.[38] The large functional groups on this lignocellulose complex, such as hydroxyl, carboxyl, carbonyl, phenol, methoxyl, quinone, and others,[39,40] make SCB possible to act as adsorption material for binding to a variety of ionic species.[41] Besides, natural fibers are also known to be incompatible with polymeric matrices due to their hydrophilic characteristic[42] and the presence of noncellulosics on their surface.[43] For this reason, chemical treatments of natural fibers are highly required, which allow the elimination of noncellulosics from their surface for more expanded applications.[44-47]

Thus, this work aimed to design new composite films based on CS and chemically modified SCB fibers to exhibit tunable release capability. First, alkali and oxidation treatments of SCB were performed to remove lignin, hemicelluloses, or both. Then, cast films were obtained by mixing different amounts of SCB derivatives into CS solution with NPK fertilizer in various loadings, intending to delineate the effects of noncellulosics on composite properties, mainly controlled release properties. For agriculture crops, complete fertilizer such as NPK provides the three most important macronutrients for the growth and development of plants.[48] Thus, the prolonged delivery of this agricultural input is particularly of interest to avoid loss during fertilization.

Experimental

Material

The SCB was gathered from the 2017 harvest (São Paulo, Brazil). Chitosan powder $(C_6H_{11}O_4)_n$ (Polymar S/A, 85% deacetylation degree and average molar mass 1.8×10^5 g mol^{-1}), glacial acetic acid, sodium hydroxide, potassium chloride, monobasic sodium phosphate, ammonium sulfate were purchased from Synth (São Paulo, Brazil). Sodium chlorite was obtained from Sigma-Aldrich (São Paulo, Brazil). Ammonia High Range reagent was purchased from Hanna (São Paulo, Brazil), Fósforo UV-PP Kit from Gold Analisa (São Paulo, Brazil), and used to determine ammonium and phosphate, respectively. All reagents were of analytical grade and used as received. The water used was from the Milli-Q water purification system (EMD, Millipore Corporate).

Preparation of fibers-derivatives from sugarcane bagasse

Holocellulose (HC), cellulignin (CL), and pure cellulose (CEL) were extracted from SCB following a two-step process to remove noncellulosic components.[49] Briefly, washed, milled, and sieved (120 μm) SCB (30 g) was treated with acidified sodium chlorite (1.4% $NaClO_2$, pH 3.5, 70 °C, 5 h) to lignin dissolution or in two repetitive alkali_washings (4% NaOH, 70 °C, 5 min) to hemicellulose removal, yielding HC and CL samples, respectively. CEL was purified by treating the HC product with alkali treatment (4% NaOH, 70 °C, 5 min, repeated twice). Derivatized SCB samples were washed with water until neutral pH, dried in an oven (60 °C), and stored in a desiccator under a vacuum for further characterization.

Adsorption capability of the SCB derivatives

The ability of the HC, CL, and CEL fibers to adsorb nitrogen (NH_4^+), phosphorous ($H_2PO_4^-$), and potassium (K^+) nutrients were systematically investigated by aqueous adsorption studies adapted from a previously reported method.[50] Briefly, each SCB derivative (50 mg) was put into 100 mL of multi-element solution at 10 mg L^{-1} of NH_4^+, $H_2PO_4^-$, and K^+ ions with vigorous shaking at pH 3.5. This process was conducted at varying ions-substrate contact times (10-60 min) to find the optimal time condition for the saturated adsorption. Suspensions were rapidly filtered at the end of time intervals to separate the phases. Finally, the collected SCB derivatives having adsorbed nutrients were dried and stored under a vacuum for further characterization.

Preparation of films

Chitosan powder (2.0 g) was solubilized into 100 mL aqueous acid acetic solution at 0.5% v/v using magnetic stirring under 25 ºC for 24 h. Next, NPK fertilizer (N-P_2O_5-K_2O mass ratio of 1:1:1) was dispersed adequately in 20 mL CS solution at loading levels of 0.1-0.4 wt.% under vigorous stirring to form homogeneous film-forming solutions. Next, the film-forming solutions were homogenized for 15 min using the Ultra Turrax disperser (15.000 rpm, IKA T 25 digital) and then poured into polystyrene Petri dishes (90 mm diameter × 15 mm deep) and dried at 60 °C for 5 h. After drying, the resulting

CS/NPK films were stored for characterizations and denoted by their fertilizer loads, i.e., 1:0.25, 1:0.5, 1:0.75, and 1:1 CS/NPK. Lastly, composite films were prepared by adding the HC, CL, or CEL fibers at 5, 10, 25, and 50 wt.% into 20 mL of 1:0.5 CS/NPK solution, followed by the same homogenization and drying procedures as already described.

Solid-state characterizations

Fourier transform infrared spectroscopy (FTIR)

FTIR samples were analyzed by grinding into KBr pellets (1:100, m/m), and the spectra were collected using a Bruker Tensor II spectrometer (Billerica, United States) in transmittance mode from an accumulation of 128 scans at 4 cm^{-1} over 4000-400 cm^{-1} region under ambient conditions.

Thermogravimetric analysis (TGA)

TGA was conducted on 5 mg of each sample at 10 °C min^{-1} heating rate from 30 ºC up to 800 °C under purging nitrogen (50 mL min^{-1}) using a PerkinElmer TGA 4000 thermogravimetric analyzer (Waltham, United States). The derivative thermogravimetric curve (dTG) was the first derivative from the TGA data.

X-ray diffraction (XRD)

The crystalline phases of samples were determined by XRD measurement on a Rigaku MiniFlex 600 powder diffractometer (Tokyo, Japan). XRD patterns were collected at 25 ºC from 10 to 45° 2θ angles (10° min^{-1} rate) using a Cu Kα radiation (λ = 1.5406 Å), generated at 45 kV, and 40 mA filament current. The crystallinity index (CrI) was determined using equation 1[51] from the intensity of 200 peaks (2θ = 22.6°), denoted as I_{200}, and the minimum intensity between 200 and 110 peaks (2θ = 18.7°), designated as I_{am}.

$$\mathrm{CrI}\,(\%) = \frac{I_{200} - I_{am}}{I_{200}} \quad (1)$$

Scanning electron microscopy (SEM)

SCB derivatives were mounted with the conductive carbon tape, sputter-coated with gold, and then examined by FEI Inspect S50 scanning electron microscope (Hillsboro, United States) at 15 kV accelerating voltage. Elemental analysis of each sample was conducted using an EDS detector (Silicon Drift Detector (SDD) Apollo X, EDAX) coupled with the SEM with 10 kV accelerating voltage. The energy-dispersive X-ray spectroscopy (EDS) characterization of the chemical surface of samples was based on the well-established method reported previously.[52] The width measurements of SCB derivatives were obtained through ImageJ software.[53]

Adsorption capacity of SCB derivatives

The concentration of potassium, ammonium, and phosphate ions was quantified from the filtered multi-element solution. Potassium was determined by Digimed DM 62 flame emission photometer (São Paulo, Brazil), and ammonium and phosphate with appropriate reagents for the determination by Thermo scientific Genesis 10S UV-Visible spectrophotometer (Waltham, United States), as reported previously by Messa and Faez.[49] The amount of nutrient adsorbed by SCB derivatives was calculated from equation 2,[54]

$$\text{Adsorption capacity} = \frac{(c_1 - c_2)v}{m} \quad (2)$$

where adsorption capacity is the amount of ion adsorbed *per* gram of substrate (mg g^{-1}); c_1 and c_2 are the initial and final concentrations (mg L^{-1}) at time t (min), respectively; v (mL) is the volume of multi-element solution; and m (g) is the mass of SCB derivative. All derivatives ranged 15-115 µm wide and hundreds of micrometers long. The averages and standard deviations were obtained from three measurements under the same conditions.

Size and organoleptic characteristics of films

The films sample were cut into circle pieces (17.1 ± 1.1 mm diameter and 0.31 ± 0.02 mm thickness) at different areas in the cast film. The weight of each sample was measured using a Sartorius TE214S analytical balance (Gottingen, Germany), and an MTX digital caliper measured their thickness. The average and standard deviation values were obtained from three measurements and reported. The physical appearance was evaluated by visual inspection to determine the homogeneity. The most representative pictures are shown in this work.

In-water nutrients release capacity

The ability of the films to release NH_4^+, $H_2PO_4^-$, and K^+ ions was investigated using the optimal CS/NPK sample reinforced with -HC, -CL, or -CEL. The in-water release of nutrients from films (ca. 32 ± 1 mg) was monitored by placing each into a polypropylene nonwoven sachet (7 × 5 cm) immersed in 50 mL deionized water under ambient conditions and without stirring. First, the aqueous solution was sampled at predetermined intervals to quantify the nutrient concentration. Then the sachet was transferred to another fresh 50 mL of deionized water. An average value

and standard deviation for each sample were determined from three measurements and reported.

Nutrient release mechanism and kinetics

The mechanism and parameters kinetics of the first 60% nutrient release from composite films were investigated using the Korsmeyer-Peppas model (equation 3),[55] which is commonly applied to predict the release of drugs from the polymeric materials,

$$\frac{M_t}{M_\infty} = kt^n \quad (3)$$

where Mt/M∞ is the fraction of potassium released at time t. The release system characteristic is defined as k, and n is the exponent of diffusion of the release mechanism.

Results and Discussion

Characterization of SCB derivatives from sugarcane bagasse

The FTIR spectra and TGA of SCB derivatives were compared (Figure S1, Supplementary Information (SI) section). The FTIR spectra of CL showed characteristic bands for phenolic compounds at 1515 and 834 cm^{-1}, corresponding to the aromatic skeletal vibration and aromatic C–H out-of-plane bending,[56,57] while hemicellulose carboxyl C=O and C–O stretching bands[58] at respective 1733 and 1254 cm^{-1} were eliminated. HC was synthesized by sodium chlorite delignification (1.4% $NaClO_2$, pH 3.5, 70 °C, 5 h) of SCB, resulting in pale yellow solids, possibly due to the less lignin content. Characteristics bands of hemicelluloses at 1733 and 1254 cm^{-1} were verified in HC. The absence of 1515 and 834 cm^{-1} bands corresponding to phenolic components significantly reduced to barely observable, signifying near-complete lignin removal after delignification. Subsequently, the alkali treatment of HC turned the pale-yellow HC to white CEL and caused the disappearance of bands at 1733 and 1254 cm^{-1}, manifesting the complete removal of hemicelluloses. Additionally, this product showed characteristic bands of O–H at 3000-3600 cm^{-1}, C–H at 2900 cm^{-1}, and glycosidic C–H deformation at 897 cm^{-1}, representing pure cellulose.[52] HC, CL, and CEL exhibited an initial slight mass loss of 4-6% around 150 °C from the evaporation of adsorbed water, and then derivatives lost near 65-70% mass rapidly up to 390 °C, corresponding to the decomposition of SCB components, leaving 9.7-20.6% char residue at 600 °C. The first derivative curve of SCB and HC showed an additional event corresponding to hemicellulose decomposition at around 298 °C, which decomposes at low temperatures.[59] Higher maximum degradation temperature (T_{max}) of CEL (352 °C) than SCB (329 °C), HC (347 °C), and CL (343 °C) samples is expected[60] and corroborates with the removal of both lignin and hemicellulose, as evidenced in the FTIR. The char residue of SCB was 20.6%, higher than HC (15.7%), CL (19.8%), and CEL (9.7%), indicating reduced chars with the procedures to remove the noncellulosics. Therefore, these results confirmed the presence of the respective hemicellulose in HC and lignin in CL, while none of the noncellulosics was found in CEL, providing evidence to support the formation of material with distinct chemical compositions.

SEM coupled with EDS examined the surface morphologies and elemental composition of SCB derivatives. All four products had a long fiber structure 15-115 μm wide and hundreds of micrometers long. The width of SCB fiber bundles reduced moderately from 115 ± 33 μm (Figure 1a) to 92 ± 16 μm HC and 78 ± 13 μm CL (Figures 1c, 1e) after delignification or alkali dissolution, respectively. When these procedures were combined, SCB fiber bundles became individualized, disintegrating significantly to much finer 15 ± 7 μm wide CEL (Figure 1g). Energy-dispersive X-ray spectroscopy (EDS) revealed that the surface of each derivative mainly consists of C and O; both are typical of cellulose[52] (Figures 1b, 1d, 1f, 1h), while the Si peak at 2.13 keV was only found in SCB, attributing residual silica ash. Na and Cl peaks at 1.06 and 2.18 keV correspond to the residual chemicals from chemical procedures, while the Al peak at 1.51 keV is probably from the milling step.

Adsorption capability of SCB derivatives

All three SCB derivatives exhibited adsorption capacities ranging from 1.6 to 14.6 mg *per* g toward a wide range of nutrients in soluble form, including cationic (NH_4^+, K^+) and anionic ($H_2PO_4^-$) species (Figures 2a-2c). At optimal time conditions, the maximum adsorption capacities of these derivative cellulose fibers toward K^+ were lower, ranging from 1.6 to 3.6 mg g^{-1} (Table 1), indicating some electrostatic interaction with all three fibers' surfaces. More interestingly, HC fibers showed the highest adsorption capacity for NH_4^+ (7.8 mg g^{-1}) followed by $H_2PO_4^-$ (3.0 mg g^{-1}), probably due to numerous surface polar hydroxyls and carboxyls groups from hemicellulose serving as adsorption sites. With distinct surface phenolic hydroxyl groups from lignin, CL exhibited a more substantial adsorption capacity for $H_2PO_4^-$ (14.6 mg g^{-1}), 4-5 times higher than HC and CEL. In contrast, NH_4^+ and K^+ adsorptions were lower at 2.6 and 1.6 mg g^{-1},

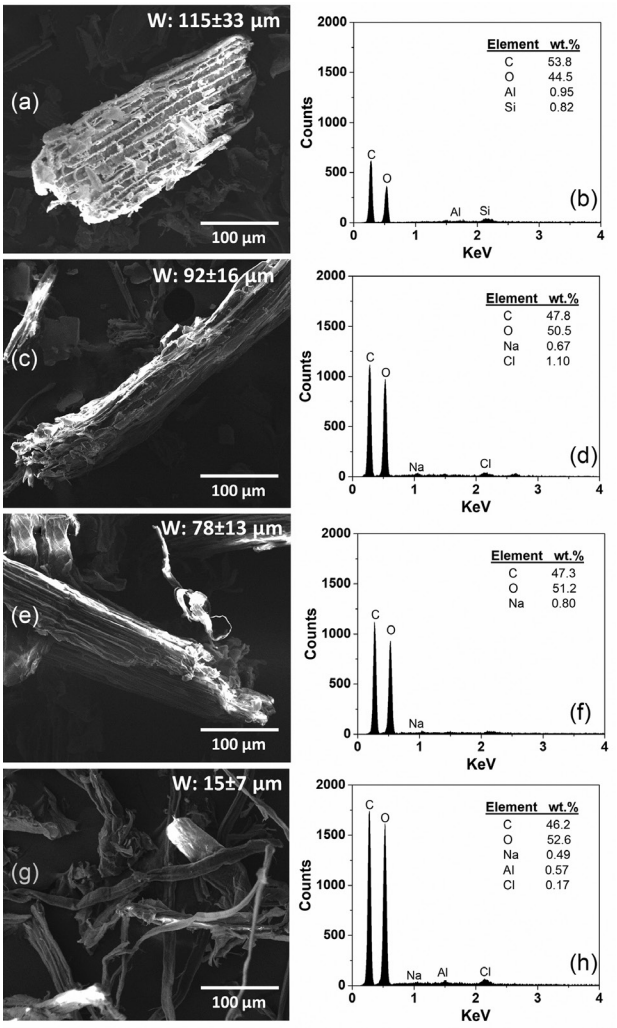

Figure 1. SEM images with elemental analysis by SEM-EDS measurement of (a, b) SCB, (c, d) HC, (e, f) CL, and (g, h) and CEL.

respectively, suggesting that phenolic compounds enormously increase the adsorption capacity of phosphorus. Even with increased specific surface area as previously observed by SEM (Figure 1g), CEL adsorption capability of 6.1, 3.9, and 2.2 mg g^{-1} for respective NH_4^+, $H_2PO_4^-$ and K^+ was intermediate to the HC and CL samples. These relatively low values are consistent with only hydroxyl groups as the significant adsorption sites from cellulose. Overall, adsorption data provide direct evidence that noncellulosics in SCB derivatives lead to a higher nutrient retention capability, which is highly desirable for material development as composites with a slowing-release property.

All SCB derivatives had similar SCB XRD patterns, i.e., with diffractions at 2θ = 14.7, 16.6, 22.6° assigned to the $1\bar{1}0$, 110, and 200 crystallographic planes in a monoclinic lattice,[61,62] maintaining the Iβ crystalline structure of cellulose after chemical (alkali and delignification procedures) and adsorption processes (Figure 2d). Additionally, no additional crystalline peaks were found after adsorption, possibly due to some interaction of ionic species with SCB derivatives, affecting the crystallization of salts. The SCB derivatives with adsorbed nutrients had CrIs values ranging from 49 to 63%, 4-12% lower than their counterparts (53-69%) (Table 1). These reduced CrIs, in essence, suggest some disorientation of cellulose crystals when ionic species are adsorbed on the SCB derivatives surface, leading to slightly less ordered structures.

Macronutrient adsorption on SCB derivatives surfaces was confirmed by EDS and nitrogen, phosphorous, and potassium mapping (Figure 3). N, P, and K peaks appeared on the spectra of all three samples after performing adsorption (Figures 3a, 3c, 3e), with weight contents of nitrogen (1.03-1.42 wt.%), phosphorous (0.22-0.30 wt.%), and potassium (0.7-0.26 wt.%). Moreover, this result may imply that the adsorption mechanism was ion-exchange between Na^+ of SCB derivatives and K^+ from the multi-elemental solution, as indicated by the disappearance of Na^+ ions after adsorption (0.49-0.80 wt.% *vs.* 0.10-0.30 wt.%). Furthermore, as shown in elemental maps (Figures 3b, 3d, 3f), all three SCB derivatives showed uniformly N (green dots), P (orange dots), and K (yellow dots) covered surfaces, again confirming that NH_4^+, $H_2PO_4^-$ and K^+ were adsorbed on the surface SCB derivatives.

In conclusion, the ability of SCB derivatives to adsorb higher and varied quantities of cationic and anionic nutrients reflects the distinct chemistry surface of fibers. Higher adsorption capacities for $H_2PO_4^-$ and NH_4^+ were significantly dependent on hydroxyl, carboxyl, or phenolic hydroxyl groups from surfaces in noncellulosic components through ion-dipole interactions. In contrast, the lower potassium adsorption driven by ion exchange was due to the scarce charged sites. Essentially, the adhesion of the ions to the SCB derivatives surface from adsorption was evident from the XRD, which may be linked to crystalline properties discussed earlier.[63]

Preparation and characterization of NPK-loaded CS films

CS solubilized completely in 0.5% v/v aqueous acetic acid under magnetic stirring for 24 h, forming a solution of CS 2 wt.%. CS solution at pH 3.9 appeared homogeneous and slightly translucent, indicating excellent solubility without agglomerates (Figure S2a, SI section). Under an acidic medium, amino groups ($-NH_2$) are expected to be protonated and converted to $-NH_3^+$. Mixing NPK with CS solution at 0.25, 0.5, 0.75, or 1:1 NPK/CS mass ratios caused slight opacity (Figure S2b), probably due to electrostatic interactions between protonated amine groups of CS and anionic species from NPK, including sulfate (SO_4^{2-}), dihydrogen phosphate ($H_2PO_4^-$) and chloride (Cl^-)

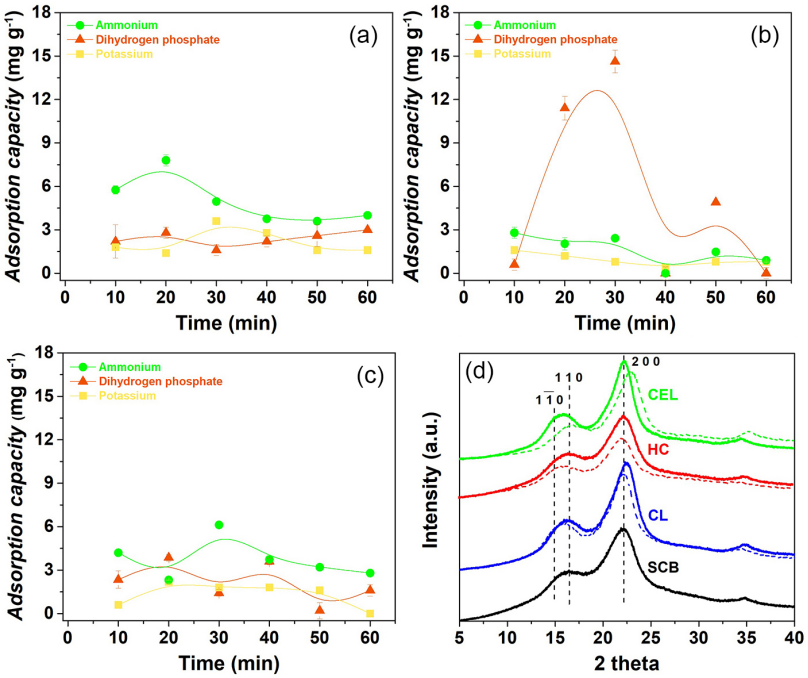

Figure 2. Characteristics of SCB derivative: adsorption capacity of (a) HC, (b) CL, and (c) CEL fibers for ammonium (NH_4^+), dihydrogen phosphate ($H_2PO_4^-$), and potassium (K^+) ions at varying ions-substrate contact times (10-60 min); (d) XRD patterns before (full line) and after (dashed line) adsorption process.

Table 1. Saturated adsorption and crystalline properties

Sample	Maximum adsorption capacity / (mg g^{-1})			CrI / %	
	NH_4^+	$H_2PO_4^-$	K^+	Non-adsorbed	Adsorbed
SCB	ND	ND	ND	52	ND
HC	7.8 ± 0.40	2.8. ± 0.38	3.6 ± 0.18	53	49
CL	2.8 ± 0.37	14.6 ± 0.78	1.6 ± 0.08	66	61
CEL	6.1 ± 0.09	3.9 ± 0.22	2.2 ± 0.11	69	63

CrI: crystallinity index; SCB: sugarcane bagasse; HC: holocellulose; CL: cellulignin; CEL: pure celulose; ND: no data.

ions. CS solutions containing varied NPK loads remained homogeneous and with no precipitation, indicating the solubility of CS was not significantly affected. Pure CS solutions could be dried in an oven (60 °C, 5 h) to form slightly yellow, opaque, and uniform films (Figure S2c). However, oven-drying of 1:0.25 CS/NPK solution yielded films with a shape highly deformed macroscopically (Figure S2d). Doubling NPK loading in the CS solution led to oven-dried films of 1:0.5 CS/NPK with the most regular shape (Figure S2e). Further increasing in NPK loading to 75 and 100% did not change the general appearance of the films, but 1:0.75 and 1:1 CS/NPK had surface cracks and irregularities (Figures S2f, S2g), suggesting the capacity of film-forming during oven-drying is greatly affected by the NPK loads. Therefore, the most uniform film from 1:0.5 CS/NPK composition was selected for further studies and named simply CS/NPK from here on.

The FTIR spectra of CS/NPK showed broadband in the 3600-3000 cm^{-1} region, which is evident for overlapped N–H and O–H stretching vibrations from CS and NPK (Figure 4a). The distinct bands at 1409 and 528 cm^{-1} are assigned to the bending vibrations of NH_4^+ and O–P–O(H),[64,65] while those at 1116 and 616 cm^{-1} correspond to two vibrational modes of the SO_4^{2-} group.[66] A more prominent band in the 1200-900 cm^{-1} region is possibly from the overlapping sulfate adsorption vibrations at 1116 and 616 cm^{-1}, and the 1230-850 cm^{-1} adsorption bands belong to the glycosidic ring of the CS structure.[67] More importantly, the diminished band at 1561 cm^{-1} characteristic of N–H vibrations of protonated amines[68] confirms the electrostatic interactions between $–NH_3^+$ from CS with anionic species from NPK, consistent with the visual evidence of chemical reaction by color-changing of CS solution after fertilizer loaded.[69]

CS remained thermally stable at up to 180 °C, then showed a mass loss at 241 °C (T_{max1}), followed by another smaller decomposition event at 309 °C (T_{max2}), corresponding to degradation of the respective protonated

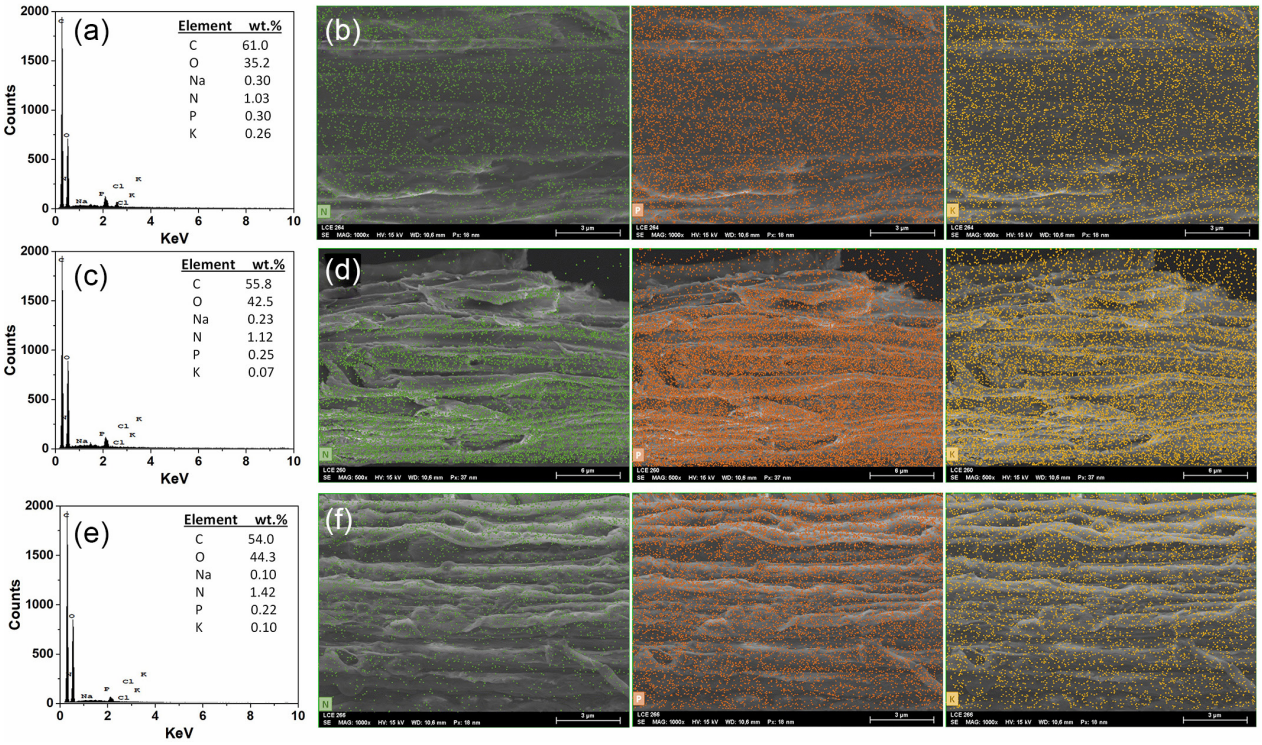

Figure 3. Elemental composition by SEM-EDS analysis with SEM secondary electron images nitrogen (green dots), phosphorous (orange dots), and potassium (yellow dots) mapping of (a, b) HC, (c, d) CL, (e, f), and CEL fibers after adsorption process.

amine and acetyl surface groups (stage I) and glucopyranose of CS (stage II),[70,71] leaving 21.1% residue at 800 °C (Figures 4b, 4d). On the other hand, CS/NPK exhibited increased thermal stability that started below 240 °C, showing more intense and separated mass loss in two stages at 286 °C (T_{max1}) and 356 °C (T_{max2}). This distinct thermal behavior suggests non-simultaneous decomposition of the chloride, sulfate and/or phosphate amines surfaces and final degradation of CS organic matter. This behavior corroborates the electrostatic interaction between the protonated amine groups of CS with anionic species of NPK. Despite NPK load, char residues of CS/NPK at

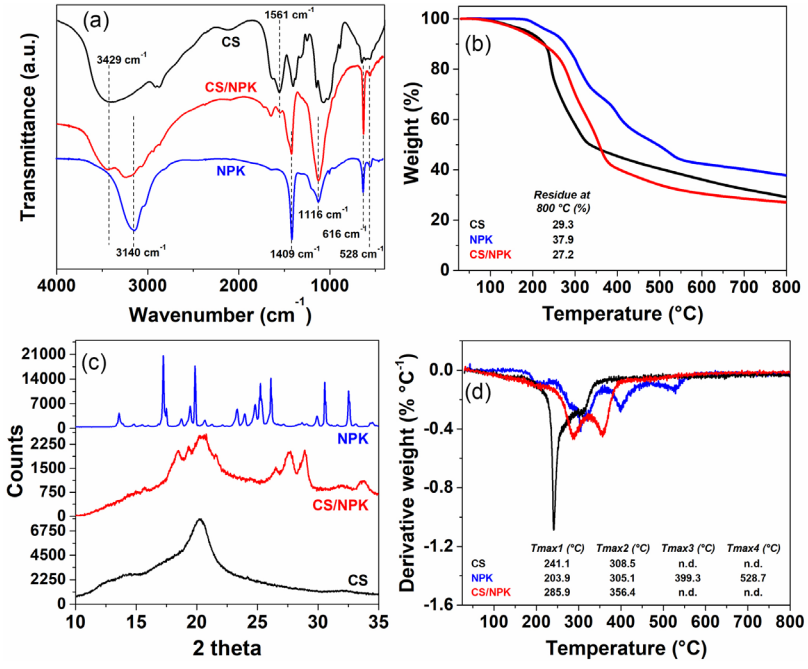

Figure 4. Characterization of CS/NPK films: (a) FTIR spectra (KBr), (b, d) TGA and dTG curves, and (c) XRD patterns.

800 °C (27.2%) were similar to CS, due to the compounds that thermally decompose below 600 °C from NPK.

X-ray diffraction of CS showed two broad peaks at 2θ = 14.3 and 20.1° belonging to the crystalline domain of CS[72] (Figure 4c). NPK exhibited several sharp, intense crystalline peaks at 2θ = 13.5, 17.2, 18.7, 19.3, 19.8, 20.6, 23.3, 23.9, 24.8, 25.2, 26.1, 29.8, 30.5, 32.5°, from the crystalline structures of KCl, $(NH_4)_2SO_4$ and NaH_2PO_4 salts that are contained in NPK fertilizer composition (Figure S3, SI section). For CS/NPK, the crystalline domain of CS in CS/NPK film remained similar to CS, but additional peaks at 2θ = 15.4, 18.1, 18.9, 21.2, 26.1, 27.3, 28.5, 33.4° were observed. As previously reported, these peaks may be attributed to the newly formed crystalline structures from the interaction between CS and NPK.[21]

CS/NPK composite films with SCB derivatives

Optimal CS/NPK film-forming reinforced with SCB derivative fiber at a different percentage (5, 10, 25, and 50 wt.%) could be cast into slightly dark yellow films. Then, adding 5-10 wt.% of fiber to the CS/NPK solution resulted in film retraction during drying, becoming denser and irregular (Figures S4a, S4b). However, increasing fiber content to 25 or 50 wt.% prevented the retraction effect and led to more regular films in shape, probably because fibers were better distributed throughout the film when higher quantities were added (Figures S4c, S4d). In addition, the augmented color intensity of composite films was consistent with increasing fiber content and closer microfibril association with the CS matrix. Therefore, considering both content fiber required and resulting film quality, the optimal condition to produce composite films was CS/NPK film reinforced with 25 wt.% fiber.

The effect of noncellulosics on the fertilizer retention ability of CS/NPK films was elucidated by in-water release studies. Normalized by weight, CS/NPK/HC, CS/NPK/CL, and CS/NPK/CEL films exhibited similar release behavior at two stages, including an initial rapid release followed by another slow and continuous one. In contrast, no change in physical integrity underwater for one week (Figure 5). CS/NPK/HC released a maximum of 64.8, 51.5, 81.7% of NH_4^+, $H_2PO_4^{2-}$, and K^+ within seven days, respectively (Figure 5a). The lowest $H_2PO_4^-$ rate released may be linked to electrostatic attractions with protonated amine groups in CS and interfacial hydrogen bonds in HC fibers, among the hydroxyls and carboxyls. In the case of the faster K^+ release rate, electrostatic attractions seem to dominate over surface interaction effects among ions potassium, CS, and HC. Meanwhile, the slowing release rate of NH_4^+ was intermediate to $H_2PO_4^-$ and K^+, probably due to its hydrogen bonding with HC fibers. In the case of CS/NPK/CL, films had different release rates for all three nutrients, in which 54.8% NH_4^+ was released slower. In contrast, 58.0% $H_2PO_4^{2-}$ and 91.5% K^+ were faster released than CS/NPK/HC films (Figure 5b), affirming the slower releasing of cationic and anionic species driven by interfacial hydrogens bonds than only electrostatic

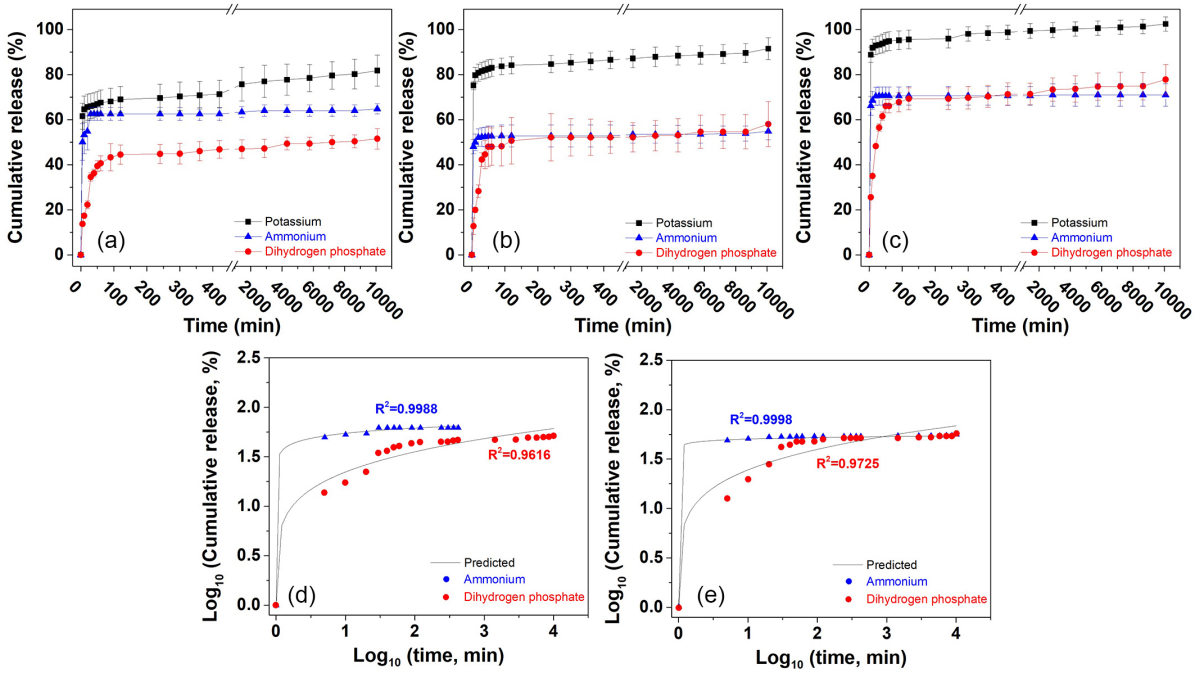

Figure 5. Cumulative release of $H_2PO_4^-$, NH_4^+, and K^+ from CS/NPK composite films with (a) HC, (b) CL, and (c) CEL fibers; and Korsmeyer-Peppas kinetic model parameters and fitting of first 60% of ammonium and dihydrogen phosphate releases and in water from (d) CS/NPK/HC and (e) CS/NPK/CL.

attractions. The release data suggest that hemicelluloses or lignin in the composite films affect fertilizer retention. In contrast, the absence of noncellulosics in composite films led to inferior release ability compared to the CS/NPK/HC and CS/NPK/CL, in which a maximum of 71.0% NH_4^+, 77.8% $H_2PO_4^-$ and 100% K^+ were substantially faster released at the same time condition (Figure 5c). These nutrient release data showed that hemicelluloses and lignin in SCB derivatives could improve nutrient retention from composite films.

Cumulative release of NH_4^+ and $H_2PO_4^-$ from CS/NPK/HC and CS/NPK/CL fitted the Korsmeyer-Peppas model well, and correlated coefficients (R^2) varied from 0.9616 to 0.9998 (Figures 5d, 5e). Composite films had a release exponent (n) lower than 0.5 for the first 60% of ammonium and dihydrogen phosphate ions released, corresponding to the *quasi*-Fickian diffusion mechanism. Therefore, the results support that these cationic and anionic nutrients diffuse through swollen and positively charged CS matrix. The slowing release of anionic and cationic nutrients was driven by attractive electrostatic forces and van der Waals interactions with protonated CS. At the same time, the noncellulosics in SCB derivatives reinforcement could improve the nutrient retention of composite films. Furthermore, their simple development approach requiring no additional chemicals or complex processes adds economic benefits to the production costs. This work demonstrates a facile and feasible strategy to explore naturally abundant polysaccharides and feedstocks as composite films with the slowing-release capability of NPK fertilizer for the first time to our knowledge.

Conclusions

The SCB derivatives (holocellulose, cellulignin, and cellulose) were evaluated as K^+, NH_4^+, and $H_2PO_4^-$ adsorption properties to increase the release properties of CS and SCB derivatives fibers. The derivatized SCB fibers exhibited distinct morphologies with widths ranging 15-115 μm and hundreds of micrometers long. The most intriguing nutrient-adsorption behavior for HC is NH_4^+ (7.8 mg g^{-1}), whereas CL showed a more substantial adsorption capability for $H_2PO_4^-$ (14.6 mg g^{-1}). The absence of noncellulosics in CEL fibers lessened their adsorption capacity, resulting in lower adsorbed nutrients following adsorption. Composite films produced by oven-dried (60 °C, 5 h) from the optimal condition were regularly shaped with 0.31 ± 0.02 mm thickness. While NPK loading into CS solution at a moderate amount (1:0.5 CS/NPK) preserves the polymer film-forming capacity, the high fiber content of 25 or 50% prevents the film's retraction effect. Furthermore, NPK fertilizer incorporated into composite films exhibited SCB derivative chemical composition-dependent release followed by a *quasi*-Fickian diffusion mechanism in water. This work demonstrates a facile and feasible strategy to explore chemically modified fibers from SCB along with CS as composite films to chemically bind and control the releases of ammonium, dihydrogen phosphate, and potassium for the first time to our knowledge.

Supplementary Information

Supplementary data associated is available free of charge at http://jbcs.sbq.org.br as PDF file.

Acknowledgments

The authors are grateful to Sao Paulo Research Foundation - FAPESP - Brazil (2017/03980-7, 2019/08057-8 and 2019/02535-5) and Coordenação de Aperfeiçoamento de Pessoal de Nível Superior - Brazil (CAPES) - Finance Code 001 for financial support. R.F. is a CNPq researcher.

Author Contributions

Lucas Luiz Messa was responsible for the investigation, formal analysis, funding acquisition, methodology, data curation, writing-original draft, and writing - review and editing; Gabriela Aparecida Contieri for the investigation, formal analysis, data curation, methodology; Roselena Faez for the conceptualization, supervision, funding acquisition, writing - review and editing.

References

1. Farias, P. I. V.; Freire, E.; da Cunha, A. L. C.; Grumbach, R. J. D. S.; Antunes, A. M. S.; *Sustainability* **2020**, *12*, 8889. [Crossref]
2. Oliveira, M. P.; Malagolli, G. A.; Cella, D.; *Rev. Interface Tecnológica* **2019**, *16*, 489. [Link] accessed in October 2022
3. Associação Nacional para Difusão de Adubos: Estatísticas, http://anda.org.br/pesquisa_setorial/, accessed in October 2022.
4. Wu, L.; Liu, M.; *Carbohydr. Polym.* **2008**, *72*, 240. [Crossref]
5. Fertahi, S.; Ilsouk, M.; Zeroual, Y.; Oukarroum, A.; Barakat, A.; *J. Controlled Release* **2021**, *330*, 341. [Crossref]
6. Blouin, G. M.; Rindt, D. W.; Moore, O. E.; *J. Agric. Food Chem.* **1971**, *19*, 801. [Crossref]
7. Rindt, D. W.; Blouin, G. M.; Getsinger, J. G.; *J. Agr. Food Chem.* **1968**, *16*, 773.
8. Lu, P.; Zhang, M.; Li, Q.; Xu, Y.; *Polym.-Plast. Technol. Eng.* **2013**, *52*, 381. [Crossref]
9. Liang, R.; Yuan, H.; Xi, G.; Zhou, Q.; *Carbohydr. Polym.* **2009**, *77*, 181. [Crossref]

10. Jarosiewicz, A.; Tomaszewska, M.; *J. Agric. Food Chem.* **2003**, *51*, 413. [Crossref]
11. Rahman, M. H.; Das, B. K.; Miah, M. A. J.; Ahmad, H.; *Bulg. J. Agric. Sci.* **2008**, *14*, 373. [Link] accessed in October 2022
12. Liang, R.; Liu, M.; *J. Agric. Food Chem.* **2006**, *54*, 1392. [Crossref]
13. Hanafi, M. M.; Eltaib, S. M.; Ahmad, M. B.; *Eur. Polym. J.* **2000**, *36*, 2081. [Crossref]
14. Giammanco, G. E.; Sosnofsky, C. T.; Ostrowski, A. D.; *ACS Appl. Mater. Interfaces* **2015**, *7*, 3068. [Crossref]
15. Baki, M.; Abedi-Koupai, J.; *J. Appl. Polym. Sci.* **2018**, *135*, 45966. [Crossref]
16. Kay, A. N.; *Trans. Kans. Acad. Sci*. **2004**, *107*,155. [Crossref]
17. Rychter, P.; Kot, M.; Bajer, K.; Rogacz, D.; Šišková, A.; Kapušniak, J.; *Carbohydr. Polym.* **2016**, *137*, 127. [Crossref]
18. Chiaregato, C. G.; Faez, R.; *Carbohydr. Polym.* **2021**, *271*, 118419. [Crossref]
19. Versino, F.; Urriza, M.; García, M. A.; *Int. J. Biol. Macromol.* **2019**, *134*, 302. [Crossref]
20. Perez Bravo, J. J.; François, N. J.; *J. Polym. Environ.* **2020**, *28*, 2681. [Crossref]
21. Messa, L. L.; Souza, C. F.; Faez, R.; *Polym. Test.* **2020**, *81*, 106196. [Crossref]
22. dos Santos, B. R.; Bacalhau, F. B.; Pereira, T. D. S.; Souza, C. F.; Faez, R.; *Carbohydr. Polym.* **2015**, *127*, 340. [Crossref]
23. França, D.; Medina, Â. F.; Messa, L. L.; Souza, C. F.; Faez, R.; *Carbohydr. Polym.* **2018**, *196*, 47. [Crossref]
24. Messa, L. L.; Froes, J. D.; Souza, C. F.; Faez, R.; *Quim. Nova* **2016**, *39*, 1215. [Crossref]
25. Souza, J. L.; Chiaregato, C. G.; Faez, R.; *J. Polym. Environ.* **2018**, *26*, 670. [Crossref]
26. El-Naggar, A. A.; El-Salmawi, K.; Ibrahim, S. M.; *J. Macromol. Sci., Part A: Pure Appl.Chem.* **2018**, *55*, 161. [Crossref]
27. Mohammadi-Khoo, S.; Moghadam, P. N.; Fareghi, A. R.; Movagharnezhad, N.; *J. Appl. Polym. Sci.* **2016**, *133*, 1. [Crossref]
28. Thongngam, M.; McClements, D. J.; *J. Agric. Food Chem.* **2004**, *52*, 987. [Crossref]
29. Eltaweil, A. S.; Omer, A. M.; El-Aqapa, H. G.; Gaber, N. M.; Attia, N. F.; El-Subruiti, G. M.; Mohy-Eldin, M. S.; Abd El-Monaem, E. M.; *Carbohyd. Polym.* **2021**, *274*, 118671. [Crossref]
30. Kean, T.; Thanou, M.; *Adv. Drug Delivery Rev.* **2010**, *62*, 3. [Crossref]
31. Ji, M.; Li, J.; Li, F.; Wang, X.; Man, J.; Li, J.; Zhang, C.; Peng, S.; *Carbohydr. Polym.* **2022**, *281*, 119078. [Crossref]
32. Singha, N. R.; Deb, M.; Chattopadhyay, P. K. In *Biodegradable Polymers, Blends and Composites*; Rangappa, S. M.; Parameswaranpillai, J.; Siengchin, S.; Ramesh, M., eds.; Elsevier: London, 2022, p. 123. [Crossref]
33. Rinaudo, M.; *Prog. Polym. Sci.* **2006**, *31*, 603. [Crossref]
34. Miles, K. B.; Ball, R. L.; Matthew, H. W. T.; *Carbohydr. Polym.* **2016**, *139*, 1. [Crossref]
35. Abdul Khalil, H. P. S.; Saurabh, C. K.; Adnan, A. S.; Nurul Fazita, M. R.; Syakir, M. I.; Davoudpour, Y.; Rafatullah, M.; Abdullah, C. K.; Haafiz, M. K. M.; Dungani, R.; *Carbohydr. Polym.* **2016**, *150*, 216. [Crossref]
36. Trindade, W. G.; Hoareau, W.; Megiatto, J. D.; Razera, I. A. T.; Castellan, A.; Frollini, E.; *Biomacromolecules* **2005**, *6*, 2485. [Crossref]
37. Tanpichai, S.; Boonmahitthisud, A.; Soykeabkaew, N.; Ongthip, L.; *Carbohydr. Polym.* **2022**, *286*, 119192. [Crossref]
38. Rocha, G. J. M.; Nascimento, V. M.; Gonçalves, A. R.; Silva, V. F. N.; Martín, C.; *Ind. Crops Prod.* **2015**, *64*, 52. [Crossref]
39. Hajiha, H.; Sain, M. In *Biofiber Reinforcements in Composite Materials*; Faruk, O.; Sain, M., eds.; Elsevier: London, 2015, p. 525. [Crossref]
40. Akanni, A. O.; Ogbiye, A. S.; Oyekanmi, E. O.; Onakunle, O. O.; *IOP Conf. Ser.: Mater. Sci. Eng.* **2019**, *640*, 012096. [Link] accessed in October 2022
41. Khoo, R. Z.; Chow, W. S.; Ismail, H.; *Cellulose* **2018**, *25*, 4303. [Link] accessed in October 2022
42. Pereira, P. H. F.; Rosa, M. F.; Cioffi, M. O. H.; Benini, K. C. C. C.; Milanese, A. C.; Voorwald, H. J. C.; Mulinari, D. R.; *Polimeros* **2015**, *25*, 9. [Crossref]
43. Oushabi, A.; *Composites, Part B* **2019**, *174*, 107059. [Crossref]
44. Asumani, O. M. L.; Reid, R. G.; Paskaramoorthy, R.; *Composites, Part A* **2012**, *43*, 1431. [Crossref]
45. Oushabi, A.; Sair, S.; Oudrhiri Hassani, F.; Abboud, Y.; Tanane, O.; El Bouari, A.; *S. Afr. J. Chem. Eng.* **2017**, *23*, 116. [Crossref]
46. Komuraiah, A.; Kumar, N. S.; Prasad, B. D.; *Mech. Compos. Mater.* **2014**, *50*, 359. [Crossref]
47. Feng, Y.-H.; Cheng, T.-Y.; Yang, W.-G.; Ma, P. T.; He, H.-Z.; Yin, X.-C.; Yu, X.-X.; *Ind. Crops Prod.* **2018**, *111*, 285. [Crossref]
48. Galembeck, F.; Galembeck, A.; dos Santos, L. P.; *Quim. Nova* **2019**, *42*, 1199. [Crossref]
49. Messa, L. L.; Faez, R.; *Cellulose* **2020**, *2*, 10077. [Crossref]
50. Fonseca, H. C. O.; *Estudo da Remoção de Sr^{2+} de Soluções Aquosas Utilizando Fibras de Coco Bruta e Ativada com Peróxido de Hidrogênio em Meio Básico*; MSc Dissertation, University of São Paulo, São Paulo, Brazil, 2015. [Link] accessed in October 2022
51. Segal, L.; Creely, J. J.; Martin Jr., A. E.; Conrad, C. M.; *Text. Res. J.* **1959**, *29*, 786. [Crossref]
52. Lu, P.; Hsieh, Y.-L.; *Carbohydr. Polym.* **2010**, *82*, 329. [Crossref]
53. *ImageJ*, version 1.51J8; National Institutes of Health, Wayne Rasband, USA, 2018.
54. Homagai, P. L.; Ghimire, K. N.; Inoue, K.; *Bioresour. Technol.* **2010**, *101*, 2067. [Crossref]
55. Korsmeyer, R. W.; Gurny, R.; Doelker, E.; Buri, P.; Peppas, N. A.; *Int. J. Pharm.* **1983**, *15*, 25. [Crossref]

56. Kumar, A.; Negi, Y. S.; Choudhary, V.; Bhardwaj, N. K.; *J. Mater. Phys. Chem.* **2014**, *2*, 1. [Crossref]
57. Yang, H.; Yan, R.; Chen, H.; Lee, D. H.; Zheng, C.; *Fuel* **2007**, *86*, 1781. [Crossref]
58. Chaker, A.; Alila, S.; Mutjé, P.; Vilar, M. R.; Boufi, S.; *Cellulose* **2013**, *20*, 2863. [Crossref]
59. Mandal, A.; Chakrabarty, D.; *Carbohydr. Polym.* **2011**, *86*, 1291. [Crossref]
60. Messa, L. L.; Faez, R.; Hsieh, Y.; *Carbohydr. Polym. Technol. Appl.* **2021**, *2*, 100085. [Crossref]
61. Moon, R. J.; Martini, A.; Nairn, J.; Simonsen, J.; Youngblood, J.; *Chem. Soc. Rev.* **2011**, *40*, 3941. [Link] accessed in October 2022
62. Klemm, D.; Heublein, B.; Fink, H. P.; Bohn, A.; *Angew. Chem., Int. Ed.* **2005**, *44*, 3358. [Crossref]
63. Grząbka-Zasadzińska, A.; Ratajczak, I.; Król, K.; Woźniak, M.; Borysiak, S.; *Cellulose* **2021**, *28*, 5745. [Crossref]
64. Sánchez-Enríquez, J.; Reyes-Gasga, J.; *Ultrason. Sonochem.* **2013**, *20*, 948. [Crossref]
65. Zhenyu, L.; Jueshi, Q.; Zhongyuan, L.; Qian, L.; Qiulin, Z.; *Adv. Mater. Sci. Eng.* **2012**, *2012*, ID 968396. [Crossref]
66. Sifontes, Á. B.; Cañizales, E.; Toro-Mendoza, J.; Ávila, E.; Hernández, P.; Delgado, B. A.; Gutiérrez, G. B.; Díaz, Y.; Cruz-Barrios, E.; *J. Nanomater.* **2015**, *2015*, ID 510376. [Crossref]
67. Mauricio-Sánchez, R. A.; Salazar, R.; Luna-Bárcenas, J. G.; Mendoza-Galván, A.; *Vib. Spectrosc.* **2018**, *94*, 1. [Crossref]
68. Lawrie, G.; Keen, I.; Drew, B.; Chandler-Temple, A.; Rintoul, L.; Fredericks, P.; Grøndahl, L.; *Biomacromolecules* **2007**, *8*, 2533. [Crossref]
69. Schauer, C. L.; Chen, M. S.; Chatterley, M.; Eisemann, K.; Welsh, E. R.; Price, R. R.; Schoen, P. E.; Ligler, F. S.; *Thin Solid Films* **2003**, *434*, 250. [Crossref]
70. Susilowati, E.; Kartini, I.; Santosa, S. J.; Triyono; *IOP Conf. Ser.: Mater. Sci. Eng.* **2016**, *107*, 012041. [Crossref]
71. Stroparo, E. C.; Mollinari, K. C.; de Souza, K. V.; *Polimeros* **2018**, *28*, 400. [Crossref]
72. Aziz, S. B.; Karim, W. O.; Brza, M. A.; Abdulwahid, R. T.; Saeed, S. R.; Al-Zangana, S.; Kadir, M. F. Z.; *Int. J. Mol. Sci.* **2019**, *20* 5265. [Crossref]

Submitted: May 25, 2022
Published online: October 27, 2022